Natural Resources Canada | Ressources naturelles Canada

GEOLOGICAL SURVEY OF CANADA
OPEN FILE 8985

A comparison of 3-D inversion strategies in the investigation of the 3-D density and magnetic susceptibility distribution in the Great Bear Magmatic Zone, Northwest Territories

N. Hayward and V. Tschirhart

2023

Canada

GEOLOGICAL SURVEY OF CANADA
OPEN FILE 8985

A comparison of 3-D inversion strategies in the investigation of the 3-D density and magnetic susceptibility distribution in the Great Bear Magmatic Zone, Northwest Territories

N. Hayward and V. Tschirhart

2023

Permanent link: https://doi.org/10.4095/331954

This publication is available for free download through GEOSCAN (https://geoscan.nrcan.gc.ca/).

Recommended citation
Hayward, N. and Tschirhart, V., 2023. A comparison of 3-D inversion strategies in the investigation of the 3-D density and magnetic susceptibility distribution in the Great Bear Magmatic Zone, Northwest Territories; Geological Survey of Canada, Open File 8985, 1 .zip file. https://doi.org/10.4095/331954

Publications in this series have not been edited; they are released as submitted by the author.

ISSN 2816-7155
ISBN 978-0-660-49149-3
Catalogue No. M183-2/8985E-PDF

Abstract

The inversion of new compilations of aeromagnetic data and gravity data are employed to investigate the 3-D physical property (magnetic susceptibility and density) distribution within the Great Bear magmatic zone. The application of two different software suites (Geosoft VOXI and UBC GIF MAG3D and GRAV3D) affords a comparison of approaches and results. The magnetic susceptibility results are broadly compatible, but Geosoft VOXI enabled more detailed definition of shallow sources, due to the lower upward continuation required for a resulting smooth model. The density results were markedly different in how the model responded to the low-resolution gravity data, in characterization of the near-surface. GRAV3D extrapolated shallow sources to surface, whereas Geosoft VOXI smoothed and closed the top of shallow sources below surface. The different magnetic susceptibility and density models can be used to assess the physical property distribution and relationships across the region. One approach, applied here, is to combine the near-surface magnetic susceptibility and density results to identify zones of coincidently high physical properties, a common physical property relationship associated with IOCG mineral deposits. These integrated models highlight many of the region's known mineral occurrences and reveal other zones for further analysis.

Introduction

The Great Bear magmatic zone (GBMZ) is a Paleoproterozoic continental magmatic arc in the Northwest Territories, Canada. The region hosts polymetallic iron oxide-copper-gold (IOCG) and iron-rich gold-cobalt-bismuth-copper deposits as well as iron oxide-apatite, albitite hosted uranium, skarn hosted tungsten and many other types of mineral prospects (Fig. 1) (e.g., Hildebrand 1986; Hildebrand et al. 1987; NORMIN database, NTGO 2012; Corriveau et al. 2010a,b, 2016, 2022a-e; Montreuil et al. 2015, 2016a, b; Potter et al. 2019).

IOCG deposits include a broad range of magnetite-, magnetite-to-hematite and hematite-group deposits, and are affiliated to an even wider range of deposit types with critical and precious metals such as iron oxide-apatite, iron-rich cobalt, skarn iron and skarn tungsten, and albitite-hosted uranium deposits (Hitzman et al. 1992; Williams et al. 2005; Corriveau et al. 2010a, 2016, 2022c,e; Williams 2010a; Porter 2010; Groves et al. 2010; Hofstra et al. 2021). Deposits form in tectonically active environments (Oliver et al. 2008; Porter 2010; Skirrow 2010; Montreuil et al., 2016a; Ootes et al., 2017) through regional metasomatism that transforms components of the upper crust into mineral systems with iron oxide alkali-calcic alteration as well as iron oxide-poor to iron-poor alteration (Corriveau et al. 2022a, c; Gadd et al. 2022), commonly with large breccia zones (Jébrak 2010).

Intense alteration results in major changes in the mineralogy, chemical composition, and physical properties of the rocks (Sandrin et al. 2009; Corriveau et al. 2010a, 2016, 2022a; Montreuil et al. 2013; Enkin et al. 2016; Blein et al. 2022). Collectively magnetite (with intense retrogression to hematite), magnetite-amphibole, magnetite-K-feldspar, biotite-magnetite, and hematite (very locally with intense retrogression to magnetite) alteration may lead to, broadly coincident, high-amplitude magnetic and gravity anomalies due to an increase in the magnetic susceptibility and density (Belperio 2007; Williams 2010b). At IOCG deposits such as at the Au-Co-Bi-Cu NICO deposit, a cobalt rich deposit with zones of IOCG mineralization located in the GBMZ, (Hayward et al. 2016), and at the IOCG Prominent Hill, and Carrapateena deposits in Australia (Belperio 2007; Porter 2010b), polymetallic mineralisation occurs in association with high gravity anomalies, spatially adjacent to, or overlapping with, high magnetic anomalies resulting from changes in alteration facies and local structure (Clarke 2014). Modeling of Australian deposits is based on high-resolution regional gravity and magnetic data

enhanced with even higher resolution at deposit-scale for a spacing varying between 100 m and 4000 m for the gravity data and 400 m for the magnetic data (Katona and Fabris 2022). Of note, even though the ore zone of the supergiant Olympic Dam deposit is ~6 km long by 3 km wide and at least 800 m deep (Fig. 10 in Corriveau et al. 2022d), the deposit footprint would not have been visible with a 10 km spaced gravity data set; it was drilled because of the proactive decision of the South Australian government to make a 6 x 6 km grid instead of the more normal 10 x 10 km grid in the 1970s (Isles 2017).

The compilation (Fig. 2, Hayward and Oneschuk 2011; Hayward and Tschirhart 2021) and interpretation of aeromagnetic, gravity and rock physical property data (Hayward et al. 2013; Hayward and Corriveau 2014; Enkin et al. 2016; Hayward et al. 2016), have provided details of the character and distribution of IOCG prospects, across what is a large area (> 50,000 km^2) of inaccessible terrain in the GBMZ. The work herein, builds on the 2-D based approaches of Hayward et al. (2013), where the magnetic, gravity and pseudo-gravity data were processed and integrated with rock physical property data to define zones of coincident high magnetic susceptibility and density. These techniques were successful in identifying zones potentially related to IOCG deposits and their alteration systems, but the range of 2-D techniques employed did not directly account for the 3-D distribution of the magnetic susceptibility and density sources.

To investigate the 3-D physical property distribution, new compilations of aeromagnetic data (Hayward and Tschirhart 2021) and gravity data are inverted to provide models of magnetic susceptibility and density contrast. Application of two geophysical inversion software suites, Geosoft VOXI Earth Modelling (Seequent 2022) and UBC GIF MAG3D and GRAV3D (Li and Oldenburg 1996, 1998), affords a comparison of approaches and results. The preferred results are used to highlight zone of mutually high magnetic susceptibility and density. Other deposit types prospective within the GBMZ systems may have abundant iron but as silicates, carbonates and sulphides which will impact significantly the geophysical footprints of the deposits (Corriveau et al. 2022c, e; Montreuil et al. 2022). The modelling conducted herein is not tailored to these deposit types.

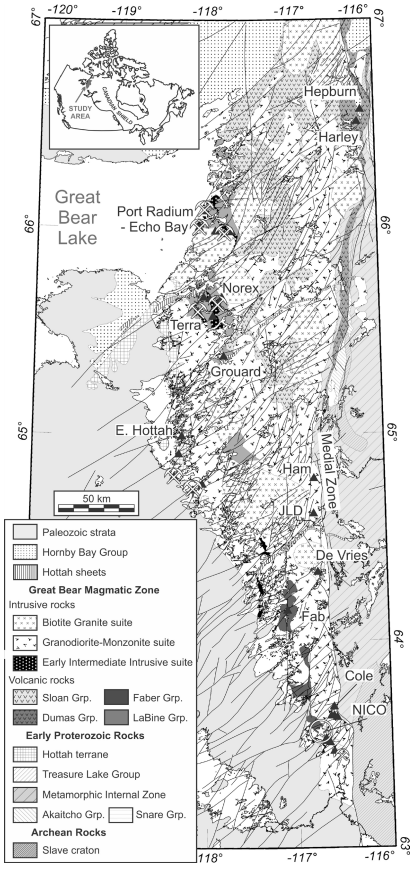

Figure 1: Location and regional geology of the Great Bear magmatic zone, Canada. Geology simplified from Hildebrand (2011), Hoffman and Hall (1993), Jackson (2008), and Gandhi et al. (2001). Black triangles show selected mineral prospects discussed in the text. Crossed hammers show the location of historical mines. Circled stars show the location of known mineral deposits. NE-striking faults derived from geophysical anomalies under the sedimentary cover to the west of the GBMZ are located on figure although they do not cut across the Paleozoic cover.

Magnetic and gravity data

Bouguer gravity data from the vicinity of the NICO deposit (Figs. 1, 2b and 3a) were gridded at 1 km cell size and levelled by 1.09 mGal prior to compilation with regional gravity data (Geological Survey of Canada 2017a). Regional gravity data were acquired by the Canadian Geodetic Survey and Geological Survey of Canada between 1944 and 2015 at a nominal station spacing of ~10 km. All data are tied to the International Gravity Standardization Network 1971 (IGSN 71; Morelli 1974). Following terrain corrections and reduction to a standard crustal Bouguer density of 2.67 g/cm^3, the data were gridded at 2 km cell size (Figs. 2b and 3a).

Aeromagnetic data, IGRF corrected and compiled from available public (Geological Survey of Canada 2017b; Hayward and Tschirhart 2021) and industry data in the vicinity of the NICO deposit. The data, initially gridded at 100 m cell size, provide almost complete high-resolution data coverage (Figs. 2a and 3c).

Rock physical property measurements of rocks sampled from the GBMZ (Hayward et al. 2013; Enkin et al. 2016) have a mean magnetic susceptibility of ~0.09 (SI) and a mean density of

~2.795 g/cm^3. It is noted, however, that as the majority of the rocks were sampled from highly altered and mineralized rocks (Enkin et al. 2016) they may not be representative of the regional variation.

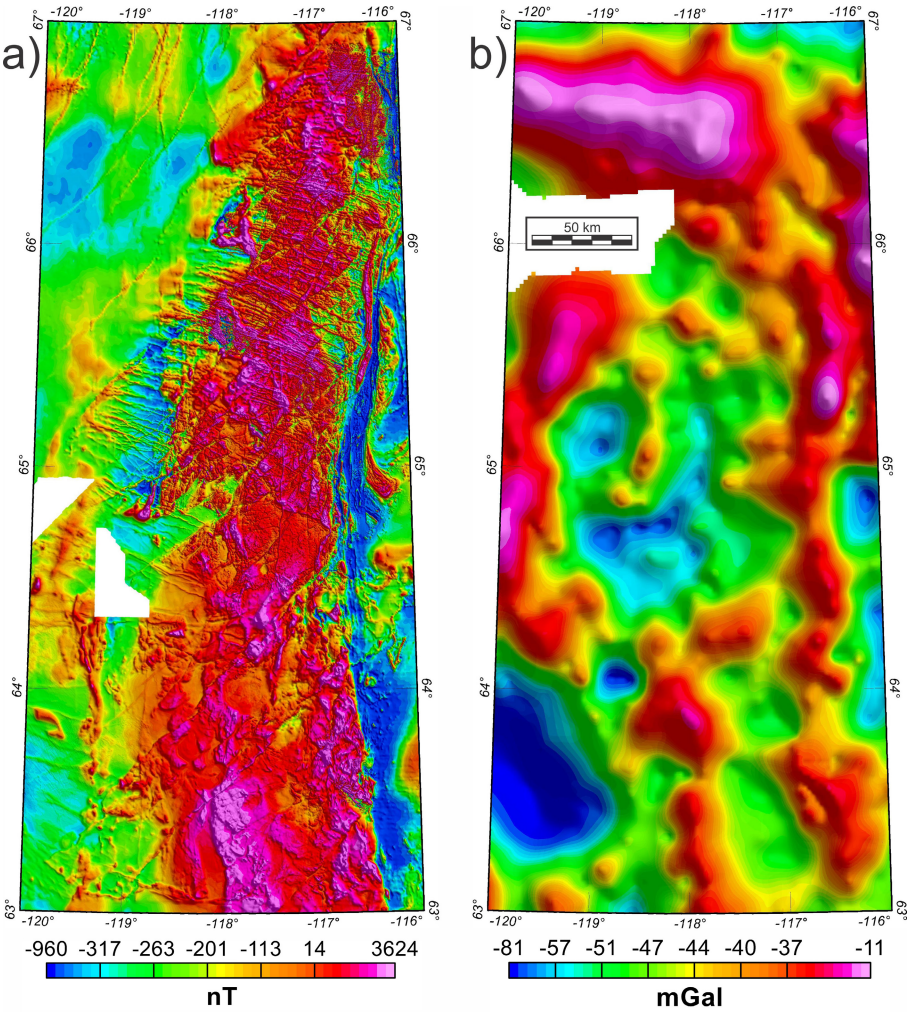

Figure 2: a) Aeromagnetic data and, b) Bouguer gravity data compilations for the Great Bear Magmatic Zone.

3-D inversion of gravity and magnetic data

Bouguer gravity data and aeromagnetic data were inverted to provide, respectively, models of the 3-D distribution of density and magnetic susceptibility within the GBMZ. For the study herein, the focus of these inversions was in defining the upper crustal physical property distribution, with the intention to identify zones of coincident or contrasting, density and magnetic susceptibility. Superimposed or juxtaposed zones of high density and magnetic susceptibility are often found in association with IOCG deposits (Belperio 2007; Porter 2010b; Hayward et al. 2013; Clarke 2014; Hayward et al. 2016).

To compare the effectiveness of different approaches, the gravity and magnetic data were inverted using two different software suites, the UBC GIF suite, GRAV3D and MAG3D (Li and Oldenburg 1996, 1998), and the Geosoft VOXI Earth Modelling (Seequent 2022).

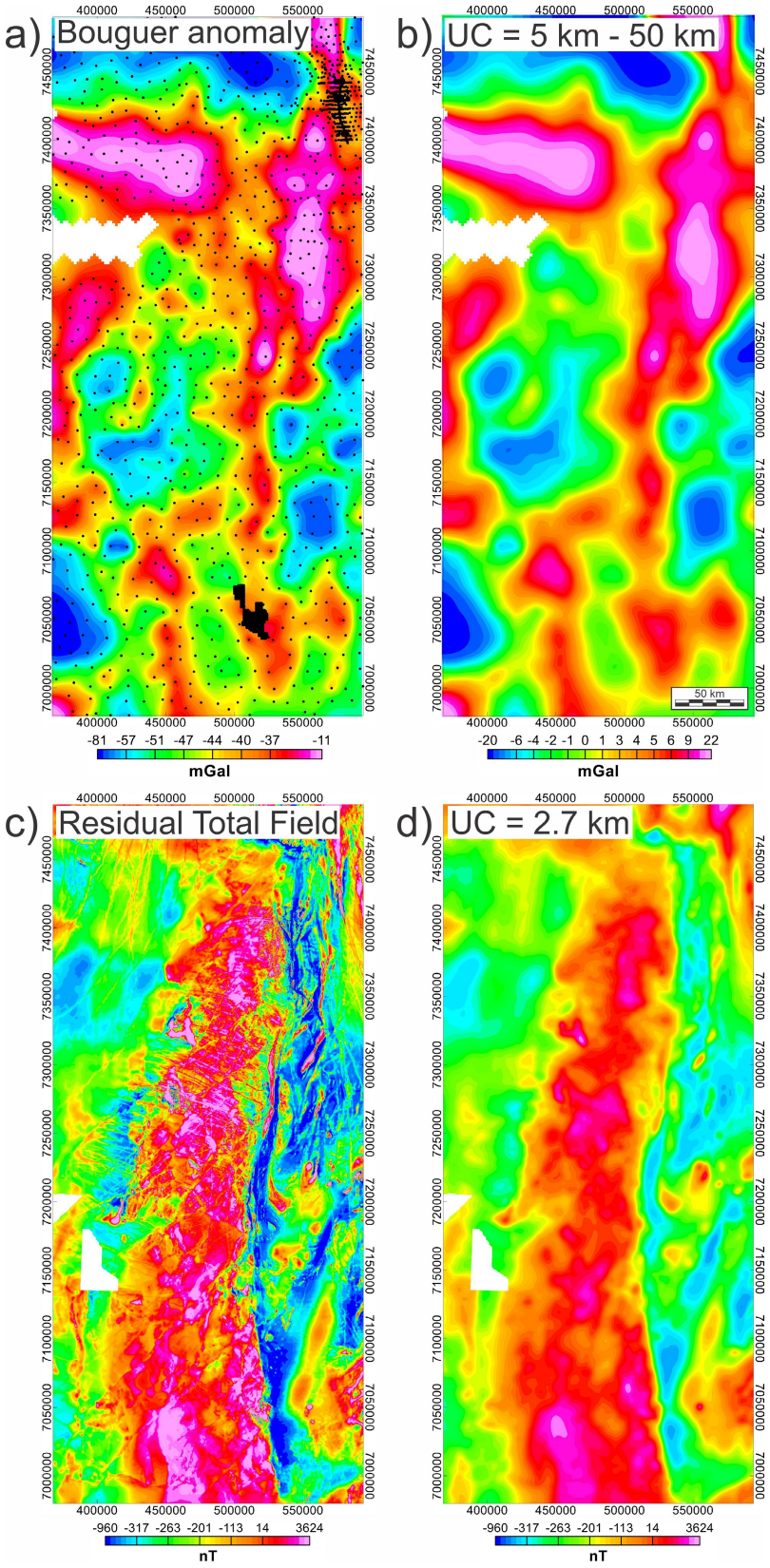

Figure 3: Potential field data for the model area, a) Bouguer gravity data for the 3-D inversion model. Black dots show station locations. b) Bouguer gravity data upward continued by 5 km and reduced through the subtraction of a version of the data upward continued by 50 km. c) Magnetic data, d) Magnetic data upward continued by 2.7 km.

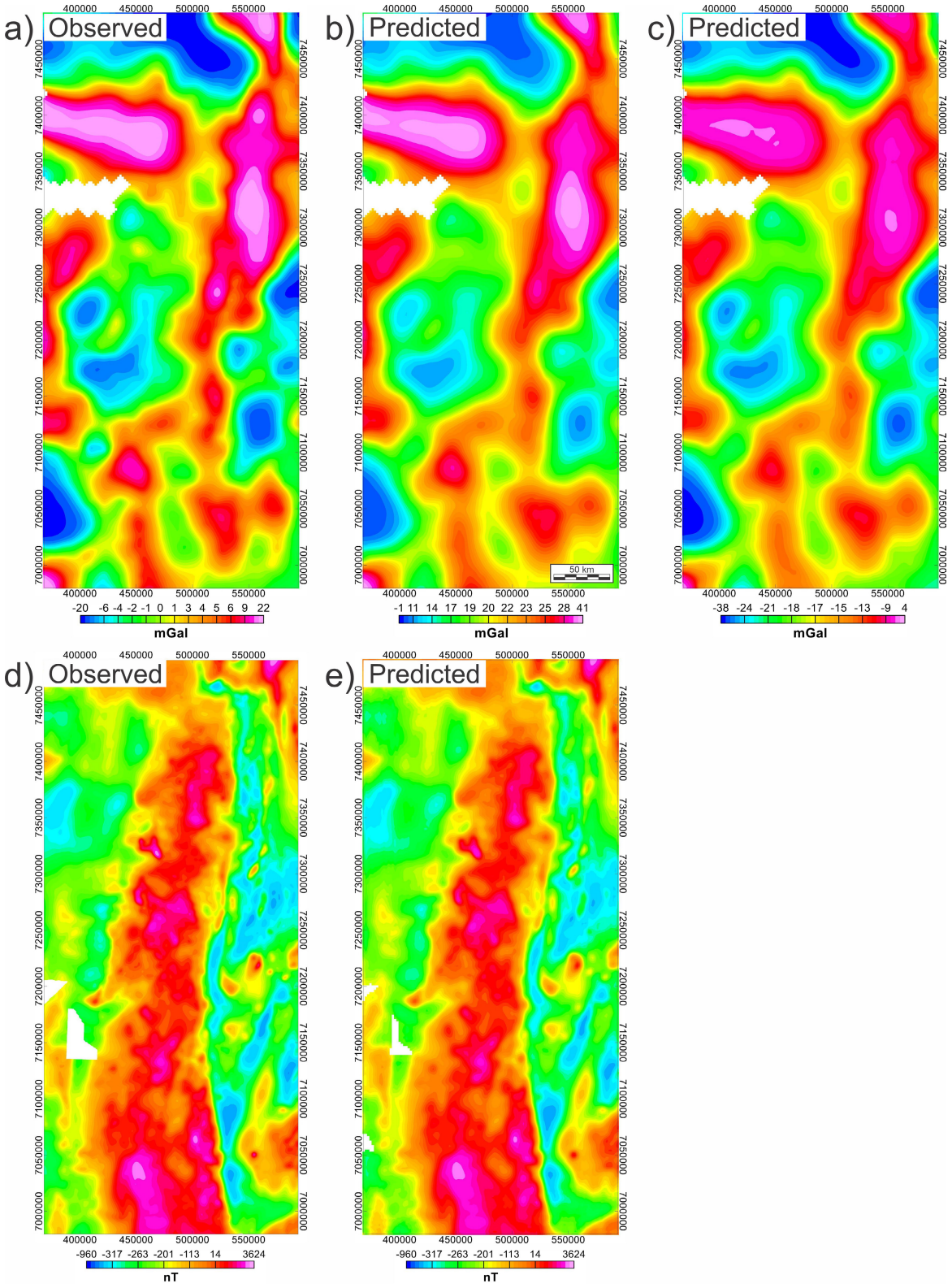

Figure 4: Observed versus Predicted anomalies from the 3-D inversion of gravity and magnetic data using the UBC GIF suite. a) Observed Bouguer anomaly, upward continued by 5 km. b) Predicted gravity anomaly for reference density of 0.3 g/cm^3. c) Predicted gravity anomaly for a reference density of -0.3 g/cm^3. d) Observed aeromagnetic anomaly, upward continued by 5 km. e) Predicted magnetic anomaly.

Gravity Inversion: UBC GIF suite, GRAV3D

Following extensive inversion model testing, the preferred gravity inversion model was constructed as follows. The model was built on a 3-D rectangular mesh with a core cell size of 5 x 5 x 1 km, determined to be a good compromise between computational size, model resolution, and artefacts. Padding to a lateral distance/depth (70/1000 km) limited artefacts at model edges. Topography was defined by a 1 km cell sized grid sampled from ETOPO1, a global relief model of Earth's surface at 1 arc-minute resolution (Amante and Eakins 2009). Bouguer gravity data were upward continued by 5 km in order to minimise shallow-sourced perturbations and noise. To isolate the upper crustal responses, the Bouguer gravity data upward continued to 50 km, were then subtracted (Figs. 3b and 4a). Bouguer data were extracted (2803 stations) from the processed grid at original station locations (Fig. 3a) and ascribed a mean error of 1 mGal.

The 3-D inversion of gravity data was performed using GRAV3D (Li and Oldenburg 1998). Therein, the inverse problem is solved by minimizing the data misfit between the observed and predicted anomaly subject to model constraints; a trade-off parameter is used to balance the data fit and model smoothness. Two models were created using reference density contrasts of 0.3 and -0.3 g/cm^3, focused on high and low density contrasts respectively (Figs. 5a, b and 6a, b). The models provide a good fit to the observed anomalies (Fig. 4), both with an RMS of 0.98 mGal.

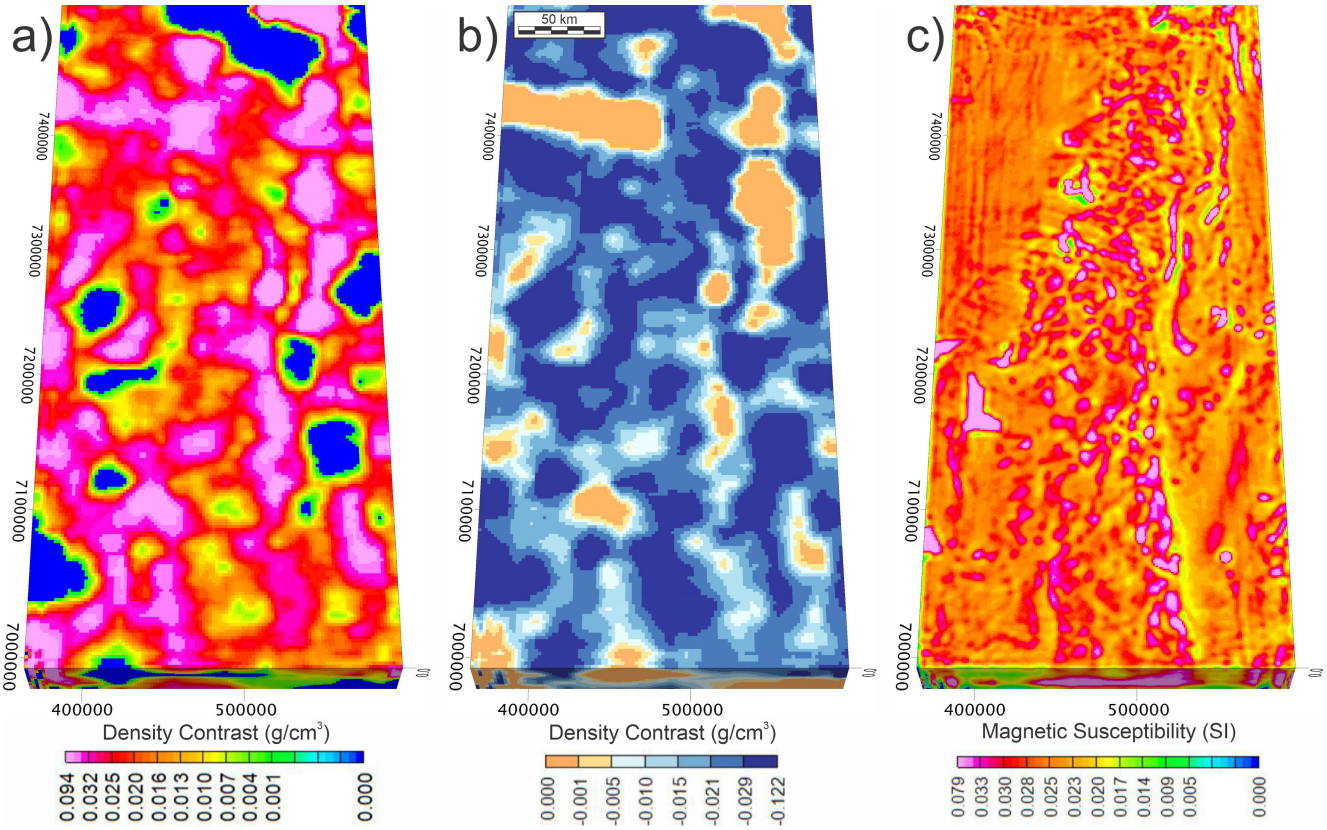

Figure 5: 3-D inversion model results for UBC GIF suite, GRAV3D and MAG3D. a) Positive density contrast (reference density = +0.3 g/cm^3) model, b) Negative density contrast (reference density = -0.3 g/cm^3) model, c) Magnetic susceptibility model (reference density = 0.03 SI).

Magnetic Inversion: UBC GIF suite, MAG3D

Following extensive inversion model testing, the preferred magnetic inversion model was constructed as follows. The model was built on a 3-D mesh with a core cell size of 1 x 1 x 1 km, determined to be a good compromise between computational size, model resolution, and artefacts. Padding to a distance/depth (70/1000 km) limited artefacts at model edges. Topography was defined by a 1 km cell sized grid sampled from ETOPO1 (Amante and Eakins 2009).

The gridded aeromagnetic data were upward continued by 2700 m to minimise shallow-sourced perturbations and noise, downsampled to a cell size of 2 km (28860 points), and ascribed a mean error of 5 nT. The magnetic field parameters were set to: inclination 82º, declination 30º, and magnetisation 59860 nT approximated from the IGRF for the time and location of data acquisition. The reference magnetic susceptibility used in the inversion was 0.03 (SI), which provided a good compromise between isolating the high susceptibility regions whilst minimizing artefacts. The model provides a good fit to the observed anomalies (Fig. 4), with an RMS of 4.98 nT.

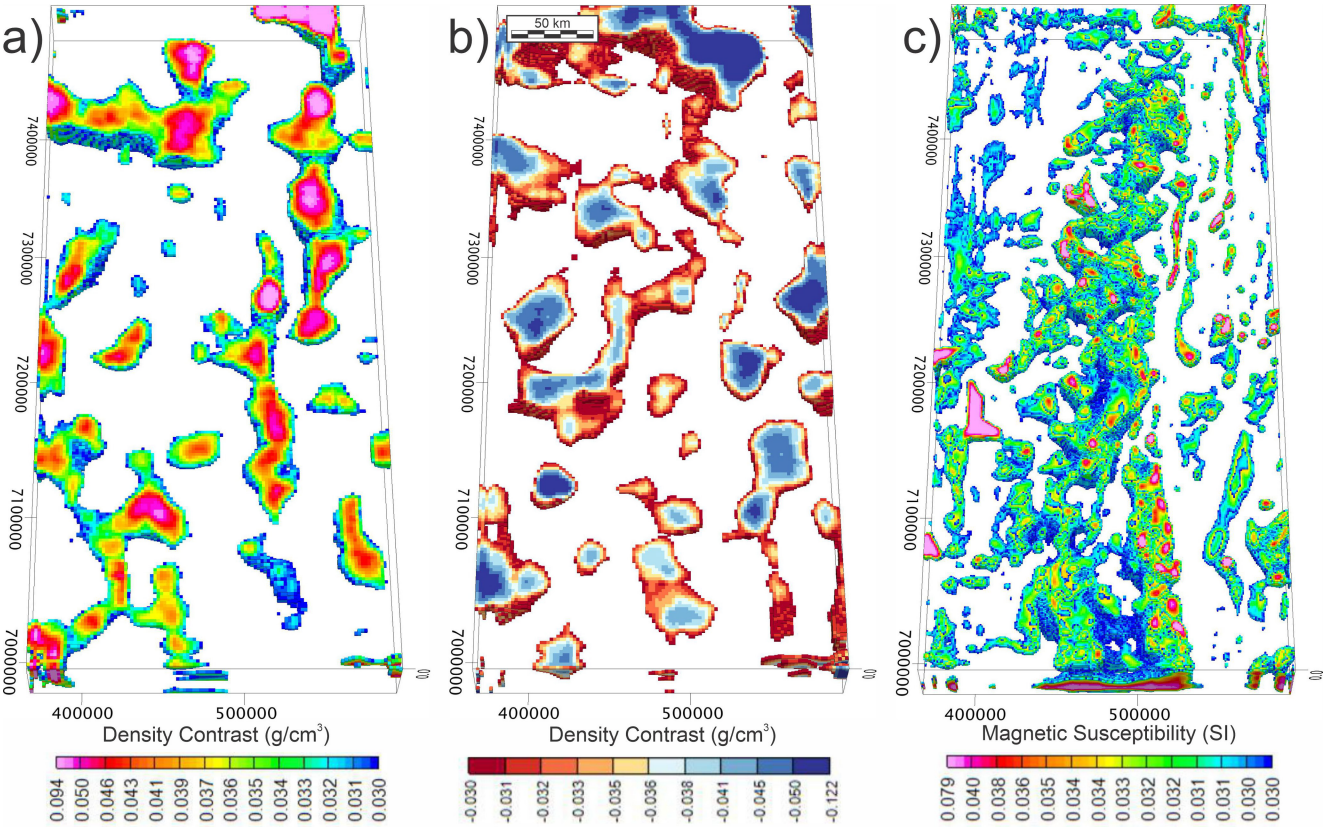

Figure 6: Windowed 3-D inversion model results for UBC-GIF inversion results for a) Positive density contrast model showing contrasts greater than 0.03 g/cm^3, b) negative density contrast model showing contrasts less than -0.03 g/cm^3, c) magnetic susceptibility model showing values of greater than 0.03 SI.

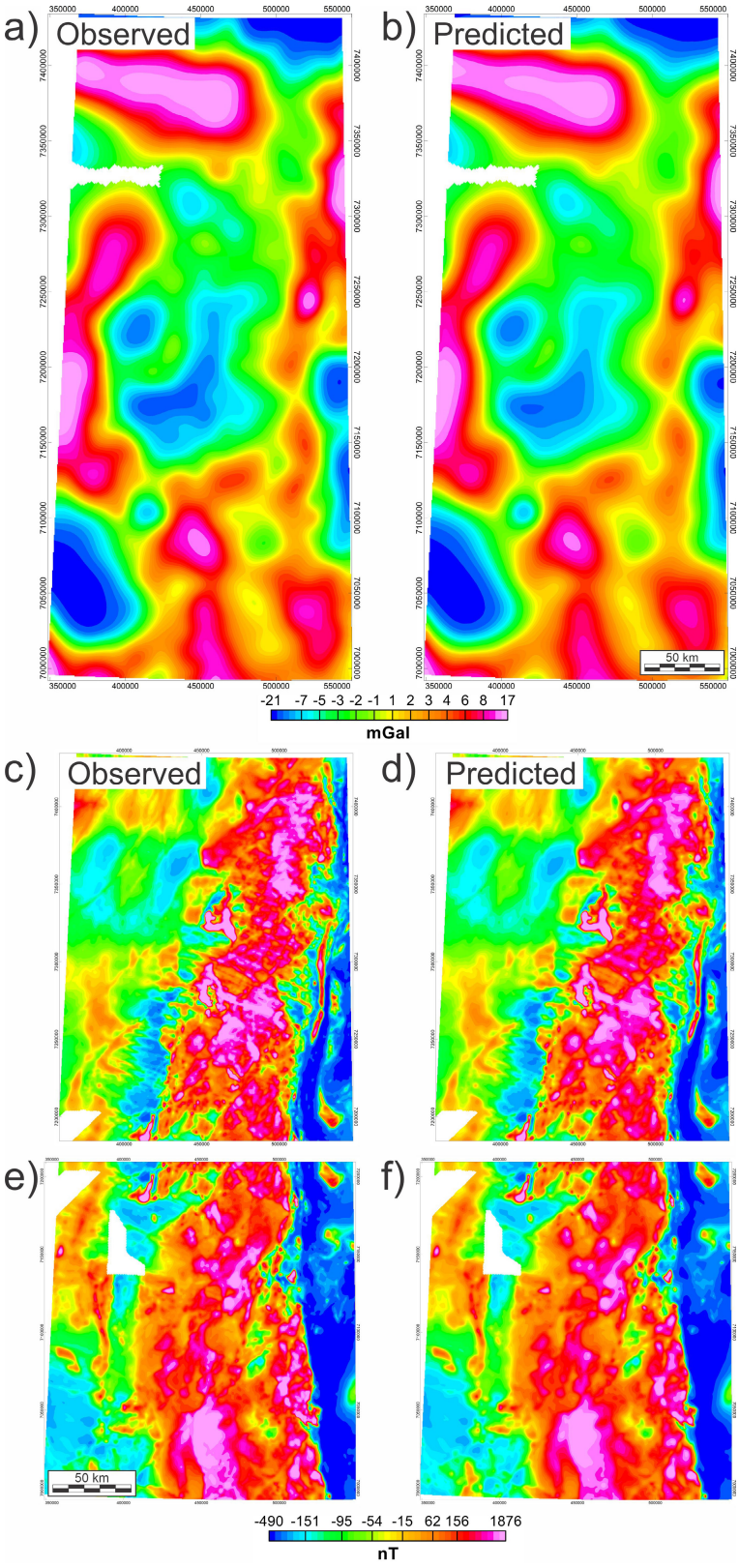

Figure 7: Observed versus predicted anomalies from the 3-D inversion of gravity and magnetic data using the VOXI. a) Observed Bouguer anomaly, upward continued by 5 km. b) Predicted gravity anomaly. c) Observed magnetic anomaly for the Northern GBMZ. d) Predicted magnetic anomaly for the Northern GBMZ. e) Observed magnetic anomaly for the Southern GBMZ. f) Predicted magnetic anomaly for Northern GBMZ.

Gravity Inversion: Geosoft VOXI Earth Modelling

Following extensive inversion and model testing, the preferred VOXI gravity inversion model was constructed as follows. The model was built using a 3D mesh with a size of 2 x 2 km. The initial z cell size was 200 m using an expansion ratio of 1.08 and extending to a depth of 40 km. Horizontal padding extended 5 cells using an expansion ratio of 1.5 and vertical padding extended 10 cells using an expansion ratio of 1.5. Topography was defined by a 1 km grid sampled from Shuttle Radar Topography Mission (SRTM) dataset.

The gridded ground gravity data was upward continued to 5 km (Fig. 5a) in order to minimise shallow-sourced perturbations and noise, ascribed a relative error of 5%, and a linear trend background was removed. No reference density model was used for the inversion and the physical property bounds were set to -1 to 1. We used the Iterative Reweighting Inversion (IRI) set to 2 to sharpen smooth inversion results and lowered the computational acceleration to 0.001 to minimise artefacts at depth that resulted when testing higher computational acceleration values. The model (Fig. 8) provided a good fit with the observed anomalies (Fig. 7a, b).

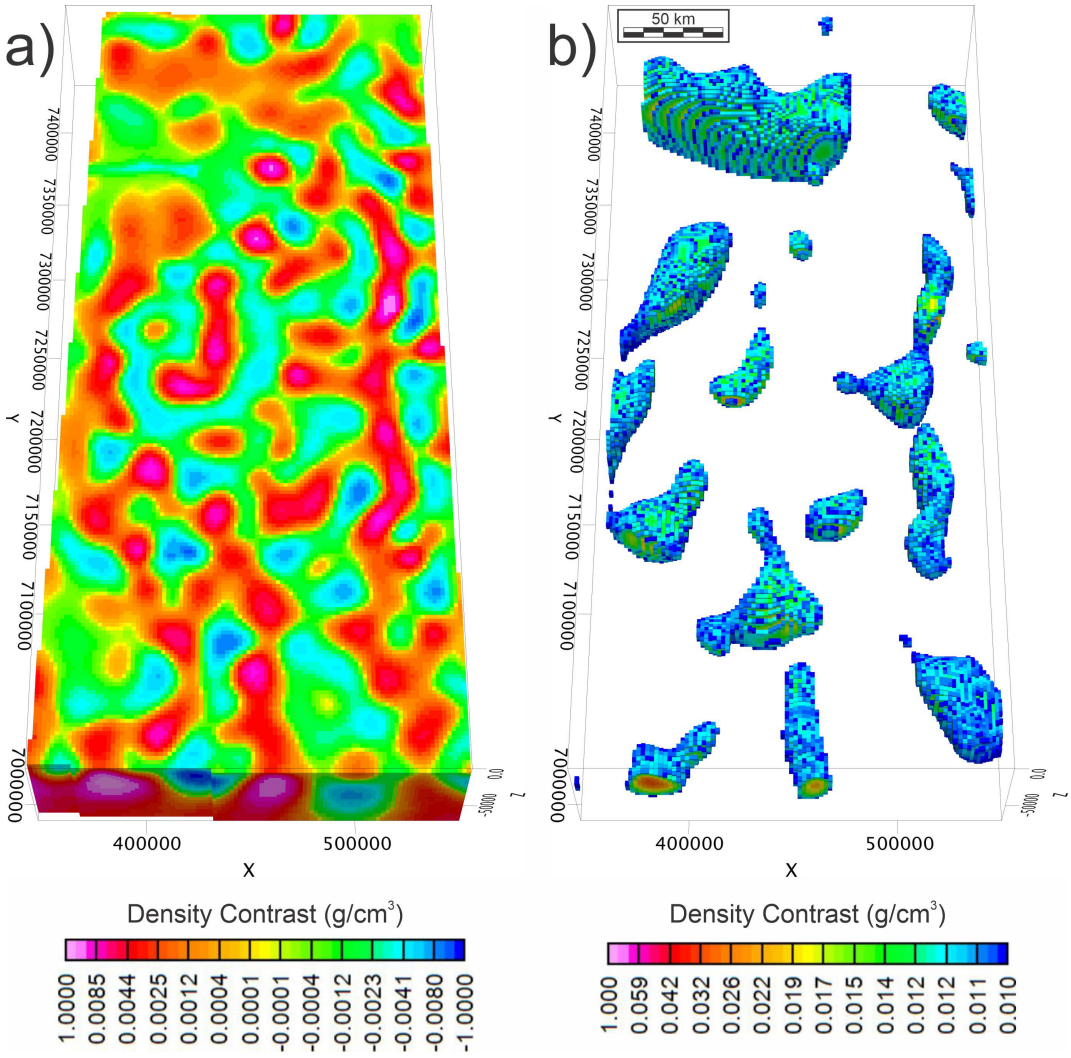

Figure 8: a) 3-D Gravity inversion results using VOXI, windowed to a depth of 5 km; b) windowed 3-D inversion model results for density values greater than 0.01 g/cm^3.

Magnetic Inversion: Geosoft VOXI Earth Modelling

Following extensive inversion and model testing, the preferred VOXI magnetic inversion model was constructed as follows. The model was built using a 3D mesh with a core size of 1 x 1 km to mimic the horizontal mesh size used for the MAG3D inversion. The initial z cell size was 250 m using an expansion ratio of 1.1 and extending to a depth of 40 km. Horizontal padding extended 5 cells using an expansion ratio of 1.5 and vertical padding extended 10 cells using an expansion ratio of 1.5. Topography was defined by a 1 km grid sampled from Shuttle Radar Topography Mission (SRTM) dataset.

The gridded aeromagnetic data was upward continued by 300 m (Fig. 7c. e) to minimise shallow-sourced perturbations and noise, and ascribed a relative error of 5%. The magnetic field parameters were set to: inclination 82.6º, declination 22.5º, and magnetisation 59133 nT and a linear trend background was removed. No reference susceptibility model was used for the inversion. We used the Iterative Reweighting Inversion (IRI) set to 2 to sharpen smooth inversion results and lowered the computational acceleration to 0.0005 to minimise artefacts at depth that resulted when testing higher computational acceleration values. The model (Fig, 9) provided a good fit with the observed anomalies (Fig. 7d, f).

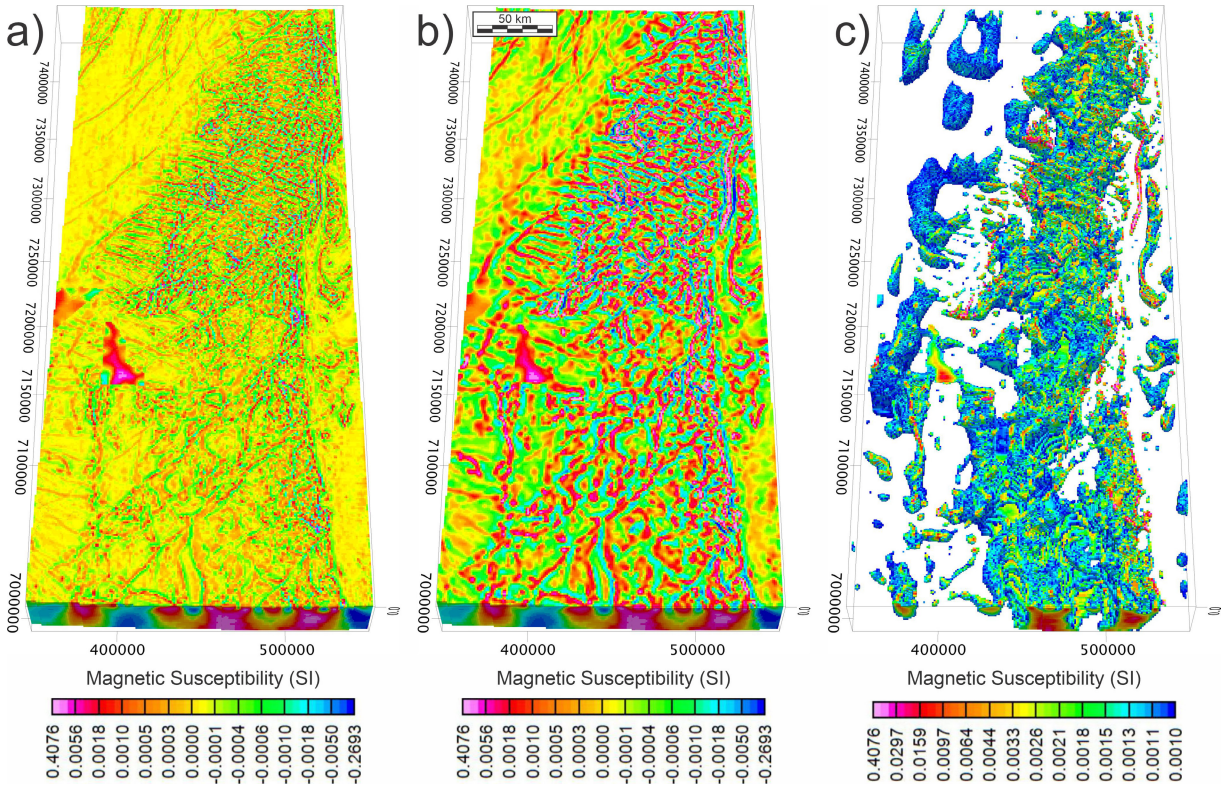

Figure 9: a) 3-D Magnetic inversion results using VOXI. b) Model clipped above a depth of 1 km. c) Model clipped above a depth of 1 km and windowed to magnetic susceptibility values greater than 0.001 SI.

Combination of magnetic susceptibility and density models

To investigate near-surface regions with coincidently high magnetic susceptibility and density contrast, model results were first clipped to a depth of 10 km and then windowed to include only their highest physical properties above a user-defined threshold. The selected magnetic susceptibility and density contrast models were then merged (Figure 10). Results using the VOXI magnetic susceptibility model (Figure 10a) provide a more detailed result than those using the MAG3D magnetic model (Figure 10b). This difference is primarily attributed to the upward continuation that was required for a smooth model result in the MAG3D inversion, which reduced the short-wavelength/near-surface magnetic signal.

The 3 density contrast models and 2 magnetic susceptibility models are provided to the reader, in both Geosoft voxel and ascii format, so that they may explore the 3-D results further. Geosoft voxels may be viewed with the Geosoft viewer, available free at https://www.seequent.com/products-solutions/geosoft-viewer/

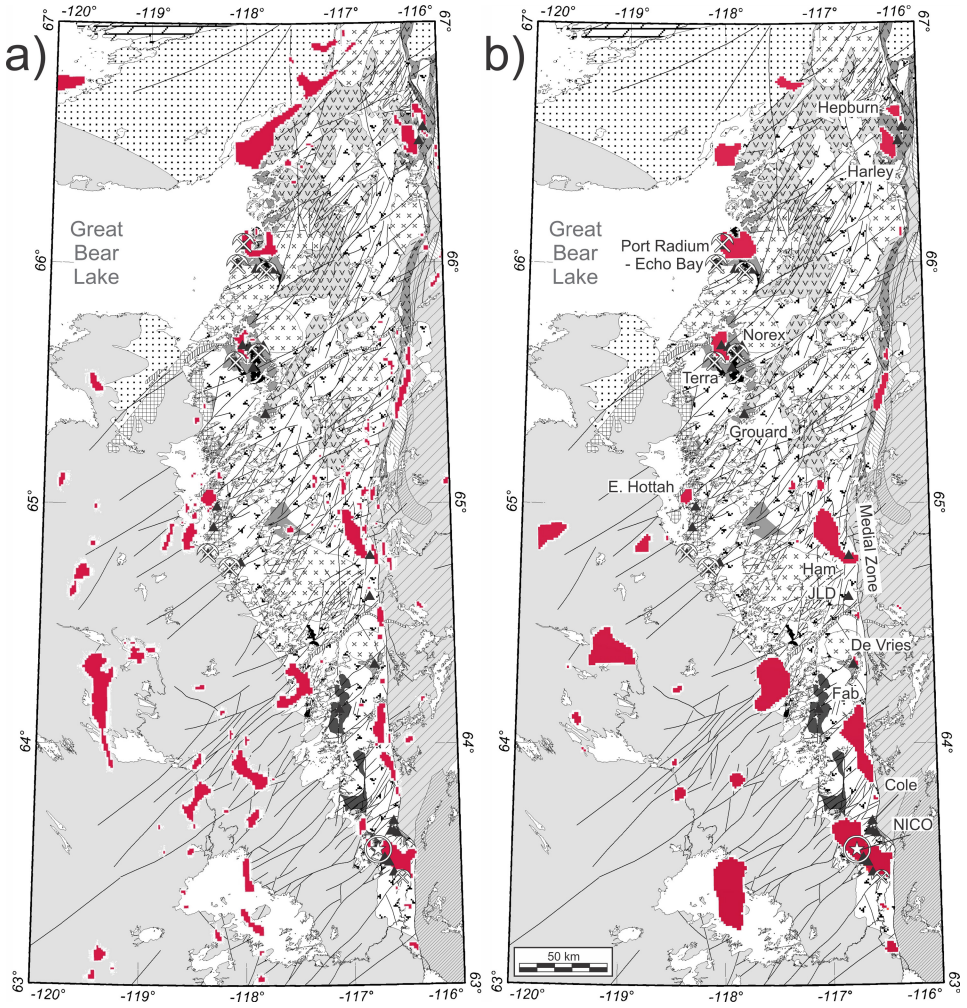

Figure 10: Regions of coincident high magnetic susceptibility and density contrast from the combination of 3-D model results (0 to 10 km depth). a) Magnetic susceptibility from the VOXI model (threshold = 0.01 SI) and density contrast from the Grad3D model (threshold = 0.03 g/cm3). b) Magnetic susceptibility from the MAG3D model (threshold = 0.0375 SI) and density contrast from the Grad3D model (threshold = 0.03 g/cm3).

Discussion

Comparison of UBC GIF Suite and VOXI model results

The magnetic susceptibility results obtained from VOXI Earth Modelling (Fig. 9) were overall similar to those from the MAG3D inversion (Fig. 6c). However, the results varied most significantly in the detail of the near-surface and at depth.

During the model testing for the VOXI magnetic inversions, an identical upward continuation distance (2700 m) to the preferred MAG3D inversion was tested. This resulted in an overly smooth inversion that only resolved major magnetic features. Small features present on the preferred MAG3D model, such as the east-northeast trending Cleaver dykes, were not present on the 2700 m upward continued VOXI model.

While the VOXI model based on 300 m of upward continuation (Fig. 9) resolved more features than the 2700 m upward continued MAG3D model (Fig. 6c), similar results could likely be achieved by using a higher upward continuation distance for the VOXI model input data- achieving such continuity would be a matter of testing different upward continuation distances.

The MAG3D model extends to 70 km in contrast to the 40 km VOXI inversion. During the initial testing of the VOXI models, a 70 km depth was used but this resulted in the model populating smooth magnetic sources at depth. A depth of 40 km was chosen as it coincides near the depth of the Moho and minimized the smooth deep sources.

While fundamentally the same features are present using both inversion codes, one cannot apply the same parameters to each grid and expect the same model result when using different codes. This is particularly true of upward continuation distances as noted above.

The density model obtained from the VOXI inversion (Fig. 8) was markedly different to that from the GRAV3D inversion (Fig. 6a, b), in response to the low spatial resolution of the gravity data (nominal station spacing of ~10 km) and the inversion's ability to define the near-surface density structure. Results from the GRAV3D inversion reveal the character of the broad variations in density across the GBMZ (Fig. 6a, b), with broad zones that are extrapolated to surface and taper with depth. Results from the VOXI inversion (Fig. 8) mimic the broad distribution of the zones of high density, but are characterized by deeper broad sources that tend to close in the near-surface.

Conclusions

The inversion of magnetic and gravity data is informative in the investigation of the 3-D physical property distribution of the region. Although the modeling software and approach can greatly impact the model results, those from both VOXI and GRAV3D/MAG3D yield comparable results that contrasted in defining a reliable interpretation. The models can also be used to define 3-D zones of coincident physical property values, such as zones of both high magnetic susceptibility and density. However, the resolution of the input data, especially the broadly spaced gravity data, limits the definition of near-surface/short-wavelength features.

Acknowledgements

We wish to thank SeyedMasoud Ansari for their review of this article and Louise Corriveau for her comments on an earlier draft of the manuscript.

References

Amante, C., and Eakins, B.W. 2009. ETOPO1 1 Arc-Minute Global Relief Model: Procedures, Data Sources and Analysis. NOAA Technical Memorandum NESDIS NGDC-24. National Geophysical Data Center, NOAA. doi:10.7289/V5C8276M [accessed October 2017].

Belperio, A., 2007. Prominent Hill: A hematite-dominated, iron oxide copper-gold system. Economic Geology 102, 1499–1510.

Blein, O., Corriveau, L., Montreuil, J.-F., Ehrig, K., Fabris, A., Reid, A., and Pal, D., 2022. Geochemical signatures of metasomatic ore systems hosting IOCG, IOA, albite-hosted uranium and affiliated deposits: a tool for process studies and mineral exploration, in: Corriveau, L., Potter, E.G. and Mumin, A.H. (Eds.), Mineral systems with iron oxide copper-gold (IOCG) and affiliated deposits. Geological Association of Canada, Special Paper 52, pp. 263–298.

Clarke, D.A., 2014. Magnetic effects of hydrothermal alteration in porphyry copper and iron-oxide copper-gold systems: A review: Tectonophysics, 624-625, 46–65.

Corriveau, L., Mumin, A.H., and Setterfield, T., 2010a. IOCG environments in Canada: Characteristics, geological vectors to ore and challenges, in: Porter, T.M. (Ed.), Hydrothermal iron oxide copper-gold and related deposits: A global perspective, volume 4-advances in the understanding of IOCG deposits. Porter Geoscience Consultancy Publishing, Adelaide, pp. 311–344.

Corriveau, L., Williams, P.J., and Mumin, A.H., 2010b. Alteration vectors to IOCG mineralization – from uncharted terranes to deposits, in: Corriveau, L., Mumin, A.H. (Eds.), Exploring for iron oxide copper-gold deposits: Canada and global analogues. Geological Association of Canada Short Course Notes, 20, pp. 89–110.

Gandhi, S.S., Mortensen, J.K., Prasad, N., and van Breemen, O., 2001. Magmatic evolution of the southern Great Bear continental arc, northwestern Canadian Shield: Geochronological constraints. Canadian Journal of Earth Sciences 38, 767–785.

Corriveau, L., Montreuil, J.-F., and Potter, E.G., 2016. Alteration facies linkages among IOCG, IOA and affiliated deposits in the Great Bear magmatic zone, Canada, in: Slack, J., Corriveau, L. and Hitzman, M. (Eds.), Proterozoic iron oxide-apatite (± REE) and iron oxide-copper-gold and affiliated deposits of Southeast Missouri, USA, and the Great Bear magmatic zone, Northwest Territories, Canada. Economic Geology, 111, 2045–2072.

Corriveau, L., Montreuil, J.-F., Blein, O., Ehrig, K., Potter, E.G., Fabris, A., and Clark, J., 2022a. Mineral systems with IOCG and affiliated deposits: Part 2 – geochemical footprints, in: Corriveau, L., Potter, E.G. and Mumin, A.H. (Eds.), Mineral systems with iron oxide copper-gold (IOCG) and affiliated deposits. Geological Association of Canada, Special Paper 52, pp. 159–204.

Corriveau, L., Montreuil, J.-F., De Toni, A.F., Potter, E.G., and Percival, J.B., 2022b. Mapping mineral systems with IOCG and affiliated deposits: A facies approach, in: Corriveau, L., Potter, E.G. and Mumin, A.H. (Eds.), Mineral systems with iron oxide copper-gold (IOCG) and affiliated deposits. Geological Association of Canada, Special Paper 52, pp. 69–111.

Corriveau, L., Montreuil, J.-F., Potter, E.G., Blein, O., and De Toni, A.F., 2022c. Mineral systems with IOCG and affiliated deposits: Part 3 – metal pathways and ore deposit model, in: Corriveau, L., Potter, E.G. and Mumin, A.H. (Eds.), Mineral systems with iron oxide copper-gold (IOCG) and affiliated deposits. Geological Association of Canada, Special Paper 52, pp. 205–245.

Corriveau, L., Montreuil, J.-F., Potter, E.G., Ehrig, K., Clark, J., Mumin, A.H., and Williams, P.J., 2022d. Mineral systems with IOCG and affiliated deposits: Part 1–metasomatic footprints of alteration facies, in: Corriveau, L., Potter, E.G. and Mumin, A.H. (Eds.), Mineral systems with iron oxide copper-gold (IOCG) and affiliated deposits. Geological Association of Canada, Special Paper 52, pp. 113–158.

Corriveau, L., Mumin, A.H., and Potter, E.G., 2022e. Iron oxide copper-gold (Ag-Bi-Co-U-REE) and affiliated deposits: introduction and overview, in: Corriveau, L., Potter, E.G. and Mumin, A.H. (Eds.), Mineral systems with iron oxide copper-gold (IOCG) and affiliated deposits. Geological Association of Canada, Special Paper 52, pp. 1–25.

Enkin, R.J., Corriveau, L., and Hayward, N., 2016. Metasomatic alteration control of petrophysical properties in the Great Bear magmatic zone (Northwest Territories, Canada), in Slack, J., Corriveau, L. and Hitzman, M., eds., Proterozoic iron oxide-apatite (± REE) and iron oxide-copper-gold and affiliated deposits of Southeast Missouri, USA, and the Great Bear Magmatic Zone, Northwest Territories, Canada. Economic Geology, v. 111, 2073-2086.

Gadd, M.G., Lawley, C.J., Corriveau, L., Houlé, M, Peter, J.M., Plouffe, A., Potter, E.G., Sappin, A.-A., Pilote, J.-L., Marquis, G., and Lebel, D., 2022. Public geoscience solution for diversifying Canada's critical mineral production. Geological Society, London, Special Publications, 526, doi.org/10.1144/SP526-2021-190.

Geological Survey of Canada. 2017a. Geoscience Data Repository for Geophysical Data, Gravity Point Data, Natural Resources Canada. http://gdr.agg.nrcan.gc.ca/gdrdap/dap/searcheng.php1 (accessed MONTH 20##).

Geological Survey of Canada. 2017b. Geoscience Data Repository for Geophysical Data, Magnetic-Radiometric-EM, Compilations, Canada-200m-MAG, Natural Resources Canada. http://gdr.agg.nrcan.gc.ca/gdrdap/dap/searcheng.php1 (accessed MONTH 20##).

Groves, D.I., Bierlein, F.P., Meinert, L.D., and Hitzman, M.W., 2010. Iron oxide copper-gold (IOCG) deposits through Earth history. Implications for origin, lithospheric setting, and distinction from other epigenetic iron oxide deposits. Economic Geology 105, 641–654.

Hayward, N., and Oneschuk, D., 2011. Geophysical series, regional geophysical compilation project, Great Bear Magmatic Zone, Northwest Territories and Nunavut, NTS 85 M and N, and 86 C, D, E, F, K and L. Geological Survey of Canada, Open File, 6835/NTGO Open File 2011-05.

Hayward, N., and Corriveau, L., 2014. Fault reconstructions using aeromagnetic data in the Great Bear magmatic zone, Northwest Territories, Canada. Canadian Journal of Earth Sciences, v. 51, p. 927-942.

Hayward, N., and Tschirhart, V., 2021. Geophysical series, regional geophysical compilation project, Great Bear Magmatic Zone, Northwest Territories and Nunavut, NTS 85 M and N, and 86 C, D, E, F, K and L. Geological Survey of Canada, Open File 6835, 2022, 2 sheets, https://doi.org/10.4095/329321

Hayward, N., Enkin, R.J., Corriveau, L., Montreuil, J-F., and Kerswill, J., 2013. The application of rapid potential field methods for the targeting of IOCG mineralisation based on physical property data, Great Bear magmatic zone, Canada. Journal of Applied Geophysics, 94, 42–58.

Hayward, N., Corriveau, L., Craven, J., Enkin, R., 2016. Geophysical signature of alteration and mineralisation envelope at the Au-Co-Bi-Cu NICO deposit, NT, Canada, in Slack, J., Corriveau, L. and Hitzman, M., eds., Proterozoic iron oxide-apatite (± REE) and iron oxide-copper-gold and affiliated deposits of Southeast Missouri, USA, and the Great Bear Magmatic Zone, Northwest Territories, Canada. Economic Geology, v. 111, p. 2087-2110.

Hildebrand, R.S., 1986. Kiruna-type deposits; their origin and relationship to intermediate subvolcanic plutons in the Great Bear magmatic zone, Northwest Canada. Economic Geology 81, 640–659.

Hildebrand, R.S., 2011. Geologic synthesis, northern Wopmay orogen/Coppermine homocline; Geological Survey of Canada Open File Map 6390 (1:500 000 scale).

Hildebrand, R.S., Hoffman, P.F., and Bowring, S.A., 1987. Tectono-magmatic evolution of the 1.9-Ga Great Bear magmatic zone, Wopmay Orogen, Northwestern Canada. Journal of Volcanology and Geothermal Research 32, 99–118.

Hitzman, M.C., Oreskes, N., and Einaudi, M.T., 1992. Geological characteristics and tectonic setting of Proterozoic iron oxide (Cu-U-Au-REE) deposits. Precambrian Research 58, 241–287.

Hoffman, P., and Hall, L., 1993. Geology, Slave craton and environs, District of Mackenzie, Northwest Territories. Geological Survey of Canada, Open File 2559; 1 sheet 1 CD-ROM.

Hofstra, A., Lisitsin, V., Corriveau, L., Paradis, S., Peter, J., Lauzière, K., Lawley, C., Gadd, M., Pilote, J., Honsberger, I., Bastrakov, E., Champion, D., Czarnota, K., Doublier, M., Huston, D., Raymond, O., VanDerWielen, S.., Emsbo, P., Granitto, M., and Kreiner, D., 2021. Deposit classification scheme for the Critical Minerals Mapping Initiative Global Geochemical Database. U.S. Geological Survey Open-File Report 2021–1049, 60 p.

Isles, D., 2017. How Bernie Milton helped Hugh Rutter with the discovery of Olympic Dam. Preview 188, 41–44.

Jackson, V.A., 2008. Preliminary geologic map of part of the Southern Wopmay Orogen (parts of NTS 86B and 86C; 2007 updates); map with descriptive notes. NWT Open Report 2008-007.

Jébrak, M., 2010. Use of breccias in IOCG(U) exploration, in: Corriveau, L., Mumin, A.H., (Eds.), Exploring for iron oxide copper-gold deposits: Canada and global analogues. Geological Association of Canada, Short Course Notes 20, pp. 79–88.

Katona, L., and Fabris, A., 2021. Defining geophysical signatures of IOCG deposits in the Olympic Copper-Gold province, South Australia, using geophysics, GIS and spatial statistics, in: Corriveau, L., Potter, E.G. and Mumin, A.H. (Eds.), Mineral systems with iron oxide copper-gold (IOCG) and affiliated deposits. Geological Association of Canada, Special Paper 52, pp. 299–313.

Li, Y., and Oldenburg, D.W. 1996. 3-D inversion of magnetic data, Geophysics, 61: 394-408.

Li, Y., and Oldenburg, D.W. 1998. "3D inversion of gravity data", Geophysics, 63: 109-119.

Morelli, C. 1974. The international gravity standardization net 1971, International Association of Geodesy, Special Publication 4, 194 p.

Montreuil, J.-F., Corriveau, L., and Grunsky, E.C., 2013, Compositional data analysis of IOCG systems, Great Bear magmatic zone, Canada: To each alteration type its own geochemical signature: Geochemistry: Exploration, Environment, Analysis, 13, 229–247.

Montreuil, J.-F., Corriveau, L., and Potter, E., 2015. Formation of albitite-hosted uranium within IOCG systems: The Southern Breccia, Great Bear magmatic zone, Northwest Territories, Canada. Mineralium Deposita, 50, 293–325.

Montreuil, J.-F., Corriveau, L., and Davis, W., 2016a. Tectonomagmatic evolution of the southern Great Bear magmatic zone (Northwest Territories, Canada) – Implications on the genesis of iron oxide alkali-altered hydrothermal systems, in: Slack, J., Corriveau, L. and Hitzman, M. (Eds.), Proterozoic iron oxide-apatite (± REE) and iron oxide-copper-gold and affiliated deposits of Southeast Missouri, USA, and the Great Bear magmatic zone, Northwest Territories, Canada. Economic Geology, 111, 2111–2138.

Montreuil, J.-F., Corriveau, L., Potter, E.G., and De Toni, A.F., 2016b. On the relation between alteration facies and metal endowment of iron oxide–alkali-altered systems, southern Great Bear magmatic zone (Canada), in: Slack, J., Corriveau, L. and Hitzman, M. (Eds.), Proterozoic iron oxide-apatite (± REE) and iron oxide-copper-gold and affiliated deposits of Southeast Missouri, USA, and the Great Bear magmatic zone, Northwest Territories, Canada. Economic Geology, 111, 2139–2168.

Montreuil, J.-F., Corriveau, L., Blein, O., Ehrig, K., Hofstra, A., Lisitsin, V., Belperio, A., Schlegel, T., Mansur, E., Conliffe, J., Sparkes, G., Zhao, X.-F., Baldwin, G., Sappin, A.-A., de Toni, A.F., Goad, R., 2022. Distribution of alteration facies, deposit types, metals, and critical minerals in metasomatic iron and alkali-calcic (MIAC) mineral systems. GAC-MAC-IAH/CNC-CSPG 2022, Abstracts v. 45, p. 160.

NTGO, 2012. NORMIN – The Northern Minerals Database. NWT Geoscience Office. http://www.nwtgeoscience.ca/normin/

Oliver, N.H.S., Butera, K.M., Rubenach, M.J., Marshall, L.J., Cleverley, J.S., Mark, G., Tullemans, F., and Esser, D., 2008. The protracted hydrothermal evolution of the Mount Isa Eastern Succession: A review and tectonic implications. Precambrian Research 163, 108–130.

Ootes, L., Snyder, D., Davis, W.J., Acosta-Góngora, P., Corriveau, L., Mumin, A.H., Montreuil, J.-F., Gleeson, S.A., Samson, I.A., and Jackson, V.A., 2017. A Paleoproterozoic Andean-type iron oxide

copper-gold environment, the Great Bear magmatic zone, Northwest Canada. Ore Geology Reviews, 81, 123–139.

Potter, E.G. Montreuil, J.-F., Corriveau, L., and Davis, W., 2019. The Southern Breccia metasomatic uranium system of the Great Bear magmatic zone, Canada: Iron oxide-copper-gold (IOCG) and albitite-hosted uranium linkages, in: Decrée, S. and Robb, L. (Eds.), Ore deposits: origin, exploration, and exploitation. Geophysical Monograph 242, American Geophysical Union, John Wiley & Sons, Inc., p. 109–130.

Porter, T.M., 2010. Current understanding of iron oxide associated-alkali altered mineralised systems. Part 1 - An overview, in: Porter, T.M., (Ed.), Hydrothermal iron oxide copper-gold and related deposits. A global perspective, volume 3, Advances in the understanding of IOCG deposits. Porter Geoscience Consultancy Publishing, Adelaide, pp. 5–32.

Sandrin, A., Eldfelt, Å., Waight, T.E., Berggren, R., and Elming, S.-Å., 2009. Physical properties and petrologic description of rock samples from an IOCG mineralized area in the northern Fennoscandian Shield, Sweden. Journal of Geochemical Exploration 103, 80–96.

Seequent, 2022. VOXI Earth Modelling. https://www.seequent.com/products-solutions/geosoft-oasis-montaj/voxi/, accessed November 10, 2022.

Skirrow, R., 2010. "Hematite-group" IOCG±U ore systems. Tectonic settings, hydrothermal characteristics, and Cu-Au and U mineralizing processes, in: Corriveau, L., Mumin, A.H., (Eds.), Exploring for iron oxide copper-gold deposits: Canada and global analogues. Geological Association of Canada, Short Course Notes 20, pp. 39–58.

Williams, P.J., Barton, M.D., Johnson, D.A., Fontbote, L., de Haller, A., Mark, G., Oliver, N.H.S., and Marschik, R., 2005. Iron oxide copper-gold deposits; geology, space-time distribution, and possible modes of origin. Economic Geology 100th Anniversary Volume, pp. 371–406.

Williams, P.J., 2010a. Classifying IOCG deposits, in: Corriveau, L., Mumin, A.H., (Eds.), Exploring for iron oxide copper-gold deposits: Canada and global analogues. Geological Association of Canada, Short Course Notes 20, pp. 13–22.

Williams, P.J., 2010b. "Magnetite-group" IOCGs with special reference to Cloncurry (NW Queensland) and Northern Sweden. Settings, alteration, deposit characteristics, fluid sources, and their relationship to apatite-rich iron ores, in: Corriveau, L., Mumin, A.H., (Eds.), Exploring for iron oxide copper-gold deposits: Canada and global analogues. Geological Association of Canada, Short Course Notes 20, pp. 23–38.